



CHORUS

This is the accepted manuscript made available via CHORUS. The article has been published as:

Randomness-induced spin-liquid-like phase in the spin- $1/2$ $J_{\{1\}}-J_{\{2\}}$ triangular Heisenberg model

Han-Qing Wu, Shou-Shu Gong, and D. N. Sheng

Phys. Rev. B **99**, 085141 — Published 28 February 2019

DOI: [10.1103/PhysRevB.99.085141](https://doi.org/10.1103/PhysRevB.99.085141)

Randomness induced spin-liquid-like phase in the spin-1/2 $J_1 - J_2$ triangular Heisenberg model

Han-Qing Wu¹, Shou-Shu Gong^{2,*} and D. N. Sheng^{1†}

¹*Department of Physics and Astronomy, California State University, Northridge 91330, USA*

²*Department of Physics, Beihang University, Beijing, 100191, China*

(Dated: January 3, 2019)

We study the effects of bond randomness in the spin-1/2 $J_1 - J_2$ triangular Heisenberg model using exact diagonalization and density matrix renormalization group. With increasing bond randomness, we identify a randomness induced spin-liquid-like phase without any magnetic order, dimer order, spin glass order, or valence-bond glass order. The finite-size scaling of gaps suggests the gapless nature of both spin triplet and singlet excitations, which is further supported by the broad continuum of dynamical spin structure factor. By studying the bipartite entanglement spectrum of the system on cylinder geometry, we identify the features of the low-lying entanglement spectrum in the spin-liquid-like phase, which may distinguish this randomness induced spin-liquid-like phase and the intrinsic spin liquid phase in the clean $J_1 - J_2$ triangular Heisenberg model. We further discuss the nature of this spin-liquid-like phase and the indication of our results for understanding spin-liquid-like materials with triangular-lattice structure.

PACS numbers: 73.43.Nq, 75.10.Jm, 75.10.Kt

I. INTRODUCTION

Frustrated quantum magnets realize a surprisingly rich place to explore the interplay between classical orders and quantum fluctuations, which may lead to novel quantum phases and unconventional quantum phase transitions¹. One of the exotic quantum states is quantum spin liquid (QSL)²⁻⁵, which breaks no spin rotational or lattice translational symmetry even at zero temperature and exhibits fractionalized quasiparticles^{6,7} with the emergent long-range entanglement⁸. Nowadays, QSL is actively sought in quantum antiferromagnets with frustrated and/or competing interactions^{3,4}, which may enhance quantum fluctuations and suppress the ordering of magnetic moments. In experiment, many spin-1/2 antiferromagnetic materials on the frustrated lattices do not show any magnetic order down to very low temperature; spin-liquid-like behaviors have also been observed in the neutron scattering, NMR, and thermal conductance measurements (see Refs. 3, 4, 5 and references therein). Theoretical studies have indeed identified QSL states in particular parameter regime for some microscopic models (see review articles Refs. 3, 4, 5). However, it remains unclear if these theoretical observed quantum states explain the widely reported spin-liquid-like behaviors in materials.

In reality, materials inevitably have defects and/or random disorder. For example, in the triangular organic salt materials such as κ -(ET)₂Cu₂(CN)₃ and EtMe₃Sb[Pd(dmit)₂]₂⁹⁻¹³, the randomness of the spin degrees of freedom has been suggested as a consequence of the random freezing of the electric-polarization degrees of freedom at low temperature¹⁴. In the kagome material herbertsmithite, the random substitution of magnetic Cu²⁺ for nonmagnetic Zn²⁺ on the adjacent triangular layer would lead to the random modification of the exchange couplings connecting the Cu²⁺ on the kagome

layer¹⁵. The randomness may enhance quantum fluctuations and thus suppresses magnetic order. Very recently, it has been proposed that the disorder even can generate long-range entanglement and thus transform a classical non-Kramers spin ice into a QSL¹⁶. The interplay among frustration, quantum fluctuations, and randomness remains a largely open question in the study of frustrated quantum magnetism, leaving the origin of the spin-liquid-like behaviors in materials an intriguing question.

The pioneer corner-stone of our understanding on randomness in quantum system is the random singlet phase in the one-dimensional (1d) Heisenberg spin model, which represents the infinite-randomness fixed-point (IRFP) in the strong-disorder renormalization group (SDRG) and is universal for a broad class of spin chains¹⁷⁻²⁰. The schematic picture of the random singlet state consists of pairs of spins which are coupled together into singlets, where the long-range singlet bonds are much weaker than the short ones and the singlet bonds cannot cross^{17,21}. Later, extended 1d chains and ladder systems with randomness have also been studied²²⁻²⁷, in which other random phases such as the quantum Griffiths phase²⁸ and the spin glass phase²⁹ have been discovered.

In two dimensions (2d), Imry and Ma gave an argument for weak randomness, which suggests that the ordered state is unstable against an arbitrarily small random field that is directly coupled to the order parameter³⁰. In the strong-randomness case, the IRFP has been found in quantum Ising model^{31,32}, disordered contact process³³, or dissipative systems³⁴. For the general 2d Heisenberg models, frustration is an intriguing ingredient that may lead to novel quantum states. For example, while the Néel antiferromagnetic order persists up to the maximal randomness in the bipartite square and honeycomb Heisenberg models without frustration^{35,36}, the numerical SDRG calculation shows a large spin for-

mation in the frustrated Heisenberg models, suggesting a spin glass fixed point³⁷. The potential effects of randomness in spin-liquid-like materials have stimulated the exact diagonalization (ED) study on the frustrated triangular, kagome, and honeycomb Heisenberg models^{14,36,38,39}, in which the disordered phases displaying no magnetic or spin glass order have been found in strong bond-randomness regime. The dynamical correlation and thermodynamic properties of the random phases could be consistent with the gapless spin liquid scenario suggested from experimental observations^{14,36,38,39}.

Recently, a new triangular spin-liquid-like material YbMgGaO₄ has been reported^{40–43}. The possible mixing of Mg²⁺ and Ga³⁺ ions in the material^{40,41,44} has stimulated further study on the randomness effects^{45–49}. More recently, another triangular-lattice compound YbZnGaO₄, which is a sister compound of YbMgGaO₄, shows some spin-glass-like behaviors which may due to the disorder and frustration effects⁵⁰. Since further-neighbor interaction in the material has been identified⁴³, the nearest-neighbor model with disorder^{14,36} may not capture the novel physics of such systems. Inspired by the experimental indications, in this paper, considering the presence of further-neighbor couplings in materials, we study the bond randomness in the $J_1 - J_2$ triangular Heisenberg model, which would be more relevant to the randomness effects in the related materials. In reality, spin-orbit coupling is strong in YbMgGaO₄ and YbZnGaO₄, which effectively induces anisotropic magnetic interactions. Nonetheless, theoretical studies have found that the microscopic model with only nearest-neighbor anisotropic interactions is always magnetically ordered^{45,46}. Competing interactions and disorder seem to be the dominant ingredients for the spin-liquid-like behavior^{43,51}. Thus here we study a simpler Heisenberg model with competing J_2 interaction and bond randomness, thus that we can use SU(2) symmetry to deal with larger systems. By using the ED and density matrix renormalization group (DMRG) calculation, we identify a randomness induced spin-liquid-like (SLL) phase that does not show any magnetic order, dimer order, spin glass order, or valence bond glass (VBG) order. The dynamical spin structure factor shows a broad continuum extending to the zero frequency, supporting the gapless excitations obtained from the finite-size gap scaling. We also find the features of entanglement spectrum in the SLL phase, which may distinguish the SLL phase and the intrinsic spin liquid phase in the $J_1 - J_2$ triangular Heisenberg model^{52–57}. The nature of this SLL phase appears to be consistent with the recently proposed 2d random singlet phase⁴⁸. Finally, we discuss the relevance to the rare-earth triangular-lattice materials YbMgGaO₄ and YbZnGaO₄.

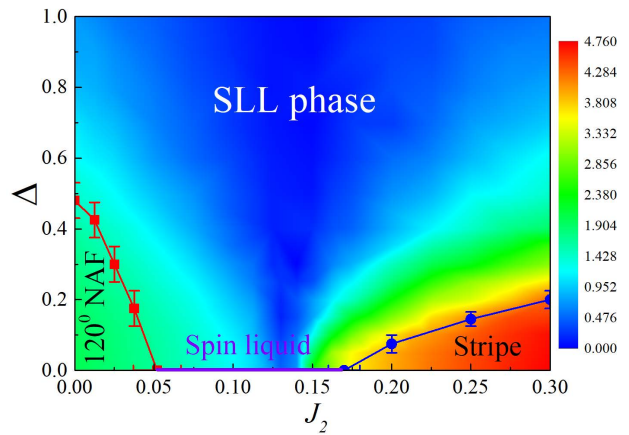


FIG. 1. Contour plot of $|S(K) - S(M)|$ in the parameter space $J_2 - \Delta$, where $S(K)$ and $S(M)$ are the spin structure factor for the 120° Néel order and the stripe magnetic order obtained on the 24-site torus system. The definition of finite-size momentum points is shown in Appendix A. The solid points with error bars denote the phase boundaries between magnetic ordered and disordered phases, where the error bars are from the linear size-scaling of magnetic order parameters shown in Fig. 2. The possible quantum phase transition between the spin liquid phase and the randomness induced spin-liquid-like (SLL) phase is discussed in section III C.

II. MODEL HAMILTONIAN AND METHODS

The Hamiltonian of the spin-1/2 $J_1 - J_2$ Heisenberg model on the triangular lattice with bond randomness reads

$$\hat{H} = \sum_{\langle ij \rangle} J_1 (1 + \Delta \cdot \alpha_{ij}) \hat{\mathbf{S}}_i \cdot \hat{\mathbf{S}}_j + \sum_{\langle\langle ij \rangle\rangle} J_2 (1 + \Delta \cdot \beta_{ij}) \hat{\mathbf{S}}_i \cdot \hat{\mathbf{S}}_j, \quad (1)$$

where α_{ij} and β_{ij} are bond random variables which are uniformly distributed in the interval $[-1, 1]$, and Δ is the parameter to control the random interval $[J_1(1 - \Delta), J_1(1 + \Delta)]$ of exchange interactions on each bond, $i = 1, 2$ for the nearest neighbor and the next-nearest neighbor. We use $\Delta \in [0, 1]$ to ensure the antiferromagnetic coupling. Here, we set $J_1 = 1$ as the energy constant.

We use ED and SU(2) DMRG^{58,59} to study this model. The finite-size clusters we used are shown in Appendix A. To measure the possible orders in the system, we define the high symmetry points in the first Brillouin zone (BZ), including the Γ point with $\mathbf{q} = (0, 0)$, the K point with $\mathbf{q} = (2\pi/3, 2\pi/\sqrt{3})$, and the M point with $\mathbf{q} = (\pi, \pi/\sqrt{3})$. While the 120° Néel order exhibits the spin structure factor peak at the K point, the stripe order has the peak at the M point. In the randomness case, we use 2000 (for smaller system sizes) to 20 (for the largest system size with the number of lattice sites $N = 48$) in ED or DMRG torus calculation, and 15 independent samples for YC6-24 and YC8-24 cylinders in DMRG calculation. We keep 2000 SU(2) states for torus

and 1200 SU(2) states for cylinder geometry in these calculations. The truncation error is less than 5×10^{-5} . In the following, we use “ $\langle \rangle$ ” and “[]” to represent quantum mechanical expectation value and stochastic averaging, respectively.

III. NUMERICAL RESULTS

A. Melting the magnetic orders

In the absence of randomness, the spin-1/2 $J_1 - J_2$ triangular Heisenberg model exhibits an intermediate spin-liquid phase for $0.07 \lesssim J_2 \lesssim 0.15$ according to the previous study⁵²⁻⁵⁷, which is sandwiched between the 120^0 Néel phase and the stripe phase. First of all, we identify the intermediate nonmagnetic phase from the vanishing magnetic orders that are extrapolated to the thermodynamic limit using the torus data up to 36 sites (see Appendix B). Our estimations qualitatively agree with the previous results although the ED data slightly overestimate the intermediate regime because of the finite-size effects. Next, we focus on the system with bond randomness.

In the magnetic order phases, bond randomness is not directly coupled with the order parameter and it has been found that only a finite bond randomness may kill the magnetic order^{14,35,36}. In order to quantitatively characterize how the ordering strength decreases with bond randomness, we introduce two magnetic order parameters: (I) square sublattice magnetization for the 120^0 Néel antiferromagnetic (NAF) phase^{14,39}

$$m_N^2 = \frac{1}{3} \sum_{\alpha=1}^3 \left[\frac{1}{(N/6)(N/6+1)} \left\langle \left(\sum_{i \in \alpha} \hat{\mathbf{S}}_i \right)^2 \right\rangle \right], \quad (2)$$

where $\alpha = 1, 2, 3$ represent the three sublattices of the 120^0 order (which is labeled by the three different colors in Appendix A). For the classical 120^0 Néel state, the spins in the same sublattice order ferromagnetically and the spins in the different sublattices are in the same plane with 120^0 angle structure. So actually we have normalized m_s^2 to 1 in the classical case by using the expectation value $(N/6)(N/6+1)$ of the total spin operator in sublattice. In quantum case, the definition of Eq. (2) describes the residual order after considering quantum fluctuations. (II) square sublattice magnetization for the stripe antiferromagnetic phase³⁹

$$m_{str}^2 = \frac{1}{2} \sum_{\beta=1}^2 \left[\frac{1}{(N/4)(N/4+1)} \left\langle \left(\sum_{i \in \beta} \hat{\mathbf{S}}_i \right)^2 \right\rangle \right], \quad (3)$$

where $\beta = 1, 2$ represent the two sublattices of the stripe order. m_{str}^2 has also been normalized to 1 in the classical stripe phase. According to the spin-wave theory⁶⁰, the

magnetic orders follow the size scaling behavior

$$m_{N/str}^2 = m_{s/str}^2(\infty) + \frac{c_1}{\sqrt{N}} + \frac{c_2}{N} + \dots \quad (4)$$

We use the leading behavior of this scaling function $1/\sqrt{N}$ to estimate the magnetic order strength in the thermodynamic limit through finite-size scaling.

In Fig. 2, we show the linear extrapolation of the magnetic orders using torus geometry up to 36 sites. To consider the two competing magnetic orders simultaneously, we choose the cluster geometries that are compatible with both the 120^0 order and the stripe order. For this reason, we only choose the 12-, 18-, 24-, and 30-site clusters for the size scaling of m_{str}^2 as shown in Fig. 2(d-f). Both orders are suppressed by increasing randomness. Up to some critical values, the bond randomness kills the magnetic orders. The system undergoes a quantum phase transition to a randomness-induced nonmagnetic phase. Then we can estimate the phase boundaries between the magnetic order phases and the nonmagnetic phase in the $J_2 - \Delta$ phase diagram of Fig. 1.

B. Randomness induced spin-liquid-like phase

In this subsection, we will focus on characterizing the SLL phase. We first show that there is no long-range chiral or dimer order. For detecting the possible orders, we define the structure factor for the scalar chiral correlation as

$$\chi(\mathbf{q}) = \frac{1}{N} \sum_{ij} e^{-i\mathbf{q}\mathbf{r}_{ij}} [\langle \hat{\chi}_i \hat{\chi}_j \rangle], \quad (5)$$

$$\hat{\chi}_i = \hat{\mathbf{S}}_i \cdot \left(\hat{\mathbf{S}}_{i+\mathbf{a}_1} \times \hat{\mathbf{S}}_{i+\mathbf{a}_2} \right),$$

and the structure factor for the dimer correlation as

$$D(\mathbf{q}) = \frac{1}{3N} \sum_{ij} \sum_{pq} e^{-i\mathbf{q}\mathbf{r}_{ip,jq}} \left[\langle \hat{\mathbf{B}}_{ip} \hat{\mathbf{B}}_{jq} \rangle \right], \quad (6)$$

$$\hat{\mathbf{B}}_{ip} = \hat{\mathbf{S}}_i \hat{\mathbf{S}}_{i+p} - \langle \hat{\mathbf{S}}_i \hat{\mathbf{S}}_{i+p} \rangle,$$

where $i+p$ means the nearest-neighbor site of i -site along $\mathbf{a}_1, \mathbf{a}_2, -\mathbf{a}_1 + \mathbf{a}_2$ direction for $p = 1, 2, 3$ respectively. \mathbf{a}_1 and \mathbf{a}_2 are the primitive vectors on the triangular lattice. $\mathbf{r}_{ip,jq}$ means the displacement between centers of two bonds, see Appendix C. In Fig. 3, we show the finite-size scaling of the peak value of the chiral and dimer structure factors. Apparently, as the bond randomness increases, these two structure factors become weaker, which do not show any ordering tendency both in the clean limit and the large randomness limit.

In magnetic systems, randomness may induce glass orders at low temperature such as the spin glass²⁹ and valence bond glass^{61,62}, which have short-range order but do not show long-range order. For example, the spin glass state has the vanished total magnetization

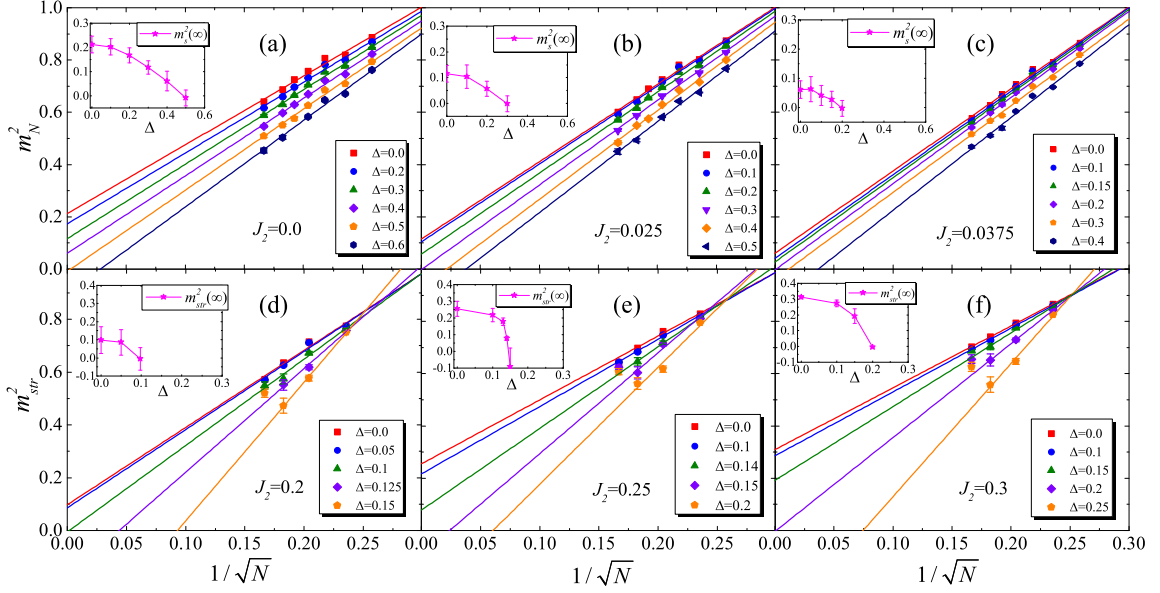


FIG. 2. (Color online) Linear extrapolation of the square magnetization of (a-c) the 120^0 Néel order and (d-f) the stripe order versus $1/\sqrt{N}$ (N is the total site number). The insets show the extrapolated order parameters as a functions of bond randomness strength Δ . The vanishing orders with bond randomness can be used to estimate the phase boundaries between the magnetic order phases and the nonmagnetic phase. In the stripe phase, the m_{str}^2 of the 36-site torus shows some deviation from other system sizes due to the finite-size geometry effects (see Appendix A).

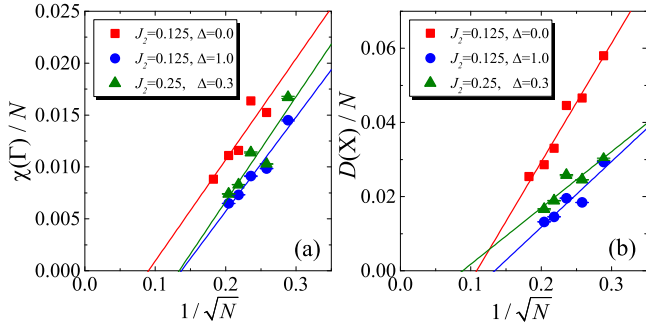


FIG. 3. (Color online) Linear extrapolation of (a) chiral and (b) dimer orders versus system size $1/\sqrt{N}$ in the nonmagnetic regime with or without bond randomness. Both orders go to zero in the thermodynamic limit. X point is the momentum point where the dimer structure factor shows the maximum value, see Appendix C.

$M = \frac{1}{N} \sum_i \langle \hat{\mathbf{S}}_i \rangle = 0$ but the nonzero spin glass order $\bar{q} = \frac{1}{N} \sum_i \langle \hat{\mathbf{S}}_i^2 \rangle \neq 0$. For detecting the possible glass order, we define the structure factor for the square spin correlation

$$G_S(\mathbf{q}) = \frac{1}{N} \sum_{ij} e^{-i\mathbf{q}\cdot\mathbf{r}_{ij}} \left[\langle \hat{\mathbf{S}}_i \hat{\mathbf{S}}_j \rangle^2 \right], \quad (7)$$

which can be used to detect the spin glass order. In our calculation, we find the peak of $G_S(\mathbf{q})$ at the Γ point with $\mathbf{q} = (0, 0)$, which is the spin-glass susceptibility and can

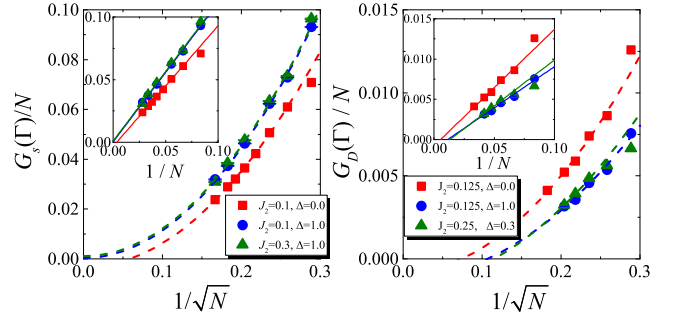


FIG. 4. (Color online) Finite-size scaling of the spin glass and valence bond glass structure factor peak. The insets show the linear extrapolation of glass orders as a function of $1/N$. The dashed lines are guides to the eye using the fitting results in the insets.

be used as spin glass order parameter^{63,64}. If the peak value increases with system size N equal to or faster than a linear behavior, the order could be finite in the thermodynamic limit. In our calculation, we find that $G_S(\Gamma)/N$ appropriately scales to zero with both $1/\sqrt{N}$ and $1/N$, as we can see in Fig. 4(a), indicating the vanished spin glass order. In the 2d Ising spin glass phase, the spin glass order scales with $\langle \bar{q}^2(L) \rangle - \langle \bar{q}^2(\infty) \rangle \propto L^{-1/2}$ ^{65–67}, which is quite different from this triangular model, where the order seems more natural to scale with $1/N$. Although the spin glass order grows slightly with increased randomness on finite-size system, the order parameter actually drops faster with increasing system size. Clearly, for both

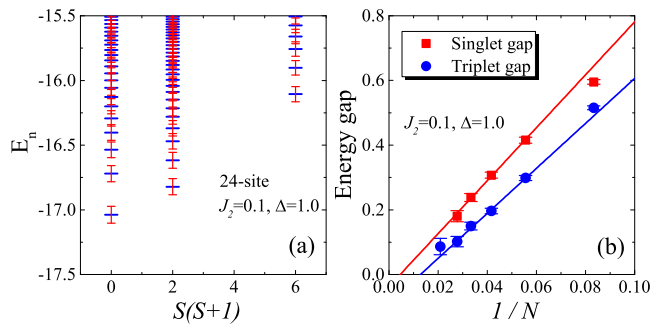


FIG. 5. (Color online) (a) Energy spectrum for $J_2 = 0.1, \Delta = 1.0$ on the 24-site torus as a function of total spin $S(S+1)$. (b) Linear scaling of the singlet and triplet gap versus $1/N$ for $J_2 = 0.1, \Delta = 1.0$.

$J_2 = 0.1, \Delta = 1.0$ and $J_2 = 0.3, \Delta = 1.0$ cases, the linearly extrapolated values are zero within numerical error. The absence of the spin glass order in the SLL phase has also been found in other frustrated Heisenberg models with bond randomness^{14,36,38}.

Similar to the spin glass order, we could define the structure factor for the VBG correlation as

$$G_D(\mathbf{q}) = \frac{1}{3N} \sum_{ij} \sum_{pq} e^{-i\mathbf{q}\mathbf{r}_{ip,jq}} \left[\langle \hat{\mathbf{B}}_{ip} \hat{\mathbf{B}}_{jq} \rangle^2 \right], \quad (8)$$

where $\hat{\mathbf{B}}_{ip}$ has been defined in Eq. (6). The VBG structure factor also shows the peak at the Γ point. Interestingly, the VBG peak at the Γ point seems to decrease with growing randomness as shown in Fig. 4(b), which indicates the absent VBG order in the SLL phase.

For further characterization of the SLL phase, we study the energy spectrum and the excitation gaps. In Fig. 5(a), we show a random averaged energy spectrum on the 24-site torus. The eigenvalues appear to be continuously distributed in the energy landscape. In both the ED torus and the DMRG cylinder calculations, the random averaged ground state is the nondegenerate spin singlet state (the ground state has probability to be in the $S = 1$ sector in some random distributions) and the averaged first excited state is the spin triplet state. In Fig. 5(b), we show that in the SLL phase both the singlet gap $\Delta_{SS} = E_1(S=0) - E_0(S=0)$ and the triplet gap $\Delta_{ST} = E_0(S=1) - E_0(S=0)$ drop fast and seem to go to vanishing, suggesting the gapless excitations.

Next, we study the dynamical spin correlation using ED simulation. We define the dynamical spin structure factor as

$$S^{zz}(\mathbf{q}, \omega) = \sum_n \left[|\langle \psi_n | \hat{S}_{\mathbf{q}}^z | \psi_0 \rangle|^2 \delta(\omega - (E_n - E_0)) \right], \quad (9)$$

where $\hat{S}_{\mathbf{q}}^z = (1/N) \sum_i e^{-i\mathbf{q}\mathbf{r}_i} \hat{S}_i^z$ is the Fourier transform of the z -component of spin operator, $|\psi_n\rangle$ is the eigenstate of the Hamiltonian with energy E_n , and $|\psi_0\rangle$ is the ground state with energy E_0 . The dynamical spin structure factor describes the correlations in both space and

time, which can be studied by inelastic neutron scattering (INS) or X-ray Raman scattering. In the Lanczos iteration method^{68,69}, the dynamical structure factor can be computed by continued fraction expansion⁷⁰ using Lanczos coefficients and rewritten as

$$\begin{aligned} S^{zz}(\mathbf{q}, \omega) &= -\frac{1}{\pi} \lim_{\eta \rightarrow 0} \text{Im} \left[\langle \psi_0 | \left(\hat{S}_{\mathbf{q}}^z \right)^\dagger \frac{1}{\omega + E_0 - \hat{H} + i\eta} \hat{S}_{\mathbf{q}}^z | \psi_0 \rangle \right], \\ &= -\frac{1}{\pi} \lim_{\eta \rightarrow 0} \text{Im} \left[\frac{\langle \psi_0 | \left(\hat{S}_{\mathbf{q}}^z \right)^\dagger \hat{S}_{\mathbf{q}}^z | \psi_0 \rangle}{z - a_0 - \frac{b_1^2}{z - a_1 - \frac{b_2^2}{z - a_2 \dots}}} \right], \end{aligned} \quad (10)$$

where $z = \omega + E_0 + i\eta$, a_i and b_{i+1} are the diagonal and sub-diagonal elements of tridiagonal Hamiltonian matrix obtained by Lanczos method with initial vector $\hat{S}_{\mathbf{q}}^z | \psi_0 \rangle$. The Lorentz broaden factor we use is $\eta = 0.02$.

In Fig. 6(a1)-(d1), we show the dynamical structure factor $S^{zz}(\mathbf{q}, \omega)$ at different J_2 along the high-symmetry path $\Gamma \rightarrow M \rightarrow K \rightarrow \Gamma$ in the large randomness case with $\Delta = 1.0$. For small J_2 , we can see a broad maxima at the K point with a low frequency, showing the short-range spin correlation dominated by the 120° Néel type. With increasing J_2 , the spectrum weight gradually transfers to the M point, which indicates the dominant stripe-like short-range correlation for $J_2 \gtrsim 0.2$. This behavior can be seen more clear from the static spin structure factor $S(\mathbf{q}) = (1/N) \sum_{ij} e^{i\mathbf{q}\mathbf{r}_{ij}} [\langle \hat{S}_i \hat{S}_j \rangle]$ shown in Fig. 6(a2)-(d2), where the broad peak at the K point transfers its weight to the M point as J_2 increases. Even with strong bond randomness, frustration seems to still affect short-range spin correlation. In the dynamical structure factor, we also find that the broad finite spectrum extends to zero frequency, supporting the gapless excitations suggested in Fig. 5(b).

For further insight into the K point and M point at the edge of the BZ, we show the dramatic changing of the dynamic spectrum as a function of randomness strength Δ in Fig. 7(a)-(b), starting from the $J_1 - J_2$ spin liquid regime. In small randomness, we see a sharp peak at the K point with the frequency $\omega \sim 0.5$, which seems to signature coherently propagating magnon excitation. Note that this sharp peak might be owing to possible strong finite-size effects^{55,57,71} in the intermediate $J_1 - J_2$ spin liquid phase. Meanwhile, the spectrum at the M point exhibits several weaker peaks. As the randomness increases, the peak at the K point transfers its weight to lower and higher frequencies, keeping a broad maxima near $\omega \sim 0.5$. On the other hand, the peak at the M point also becomes broad but shifts to the lower frequency. When the randomness is sufficiently large, a broad continuum spectrum with exponentially decaying high-frequency tail not only appears at the K and M

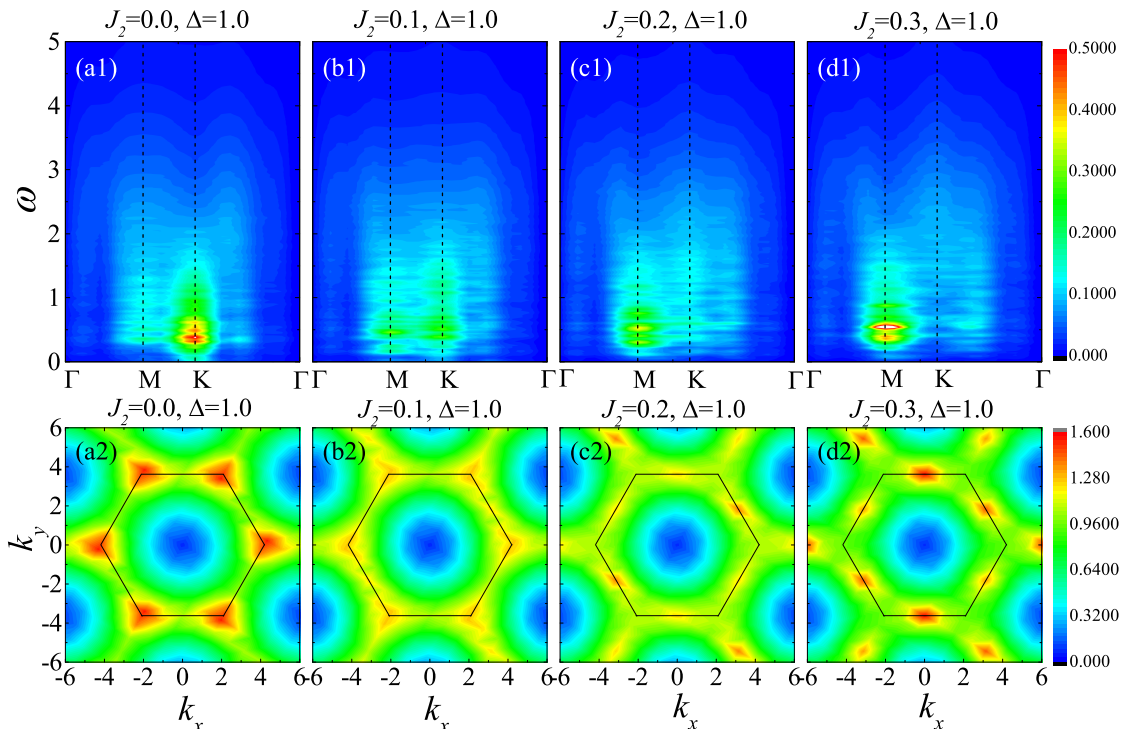


FIG. 6. (Color online) (a1)-(d1) Dynamical spin structure factor $S^{zz}(\mathbf{q}, \omega)$ along the high-symmetry path $\Gamma \rightarrow M \rightarrow K \rightarrow \Gamma$ in the momentum space. We only show the results of the 24-site cluster here. The results on other system sizes like 12 and 18 are similar to the 24-site cluster. (a2)-(d2) Static spin structure factor obtained on the YC8-24 cylinder using DMRG. We take the middle 8×8 sites in the cylinder to do the Fourier transform. As the cylinder geometry does not respect the C_6 rotation symmetry, the three M points are not equivalent.

points but also stretches to other wave vectors near the edge of the Wagner-Seitz Brillouin zone, which is quite different from the magnon-like excitations.

In order to consider the finite-size effects, we show the local or momentum integrated dynamical spin-spin correlation with different system sizes in Fig. 7 (c), which is defined as

$$S_{loc}^{zz}(\omega) = S_{ii}^{zz}(\omega) = \int d\mathbf{q} S^{zz}(\mathbf{q}, \omega) = -\frac{1}{\pi} \lim_{\eta \rightarrow 0} \text{Im} \left[\langle \psi_0 | \hat{S}_i^z \frac{1}{\omega + E_0 - \hat{H} + i\eta} \hat{S}_i^z | \psi_0 \rangle \right], \quad (11)$$

where i is the real-space lattice site. Although randomness breaks translation symmetry, it can be approximately restored if the number of random samples is large enough and thus we can take i as any lattice site. We have also calculated the local dynamical dimer correlation in Fig. 7 (d), which is defined as

$$D_{ii}(\omega) = -\frac{1}{\pi} \lim_{\eta \rightarrow 0} \text{Im} \left[\langle \psi_0 | \hat{\mathbf{B}}_i^\dagger \frac{1}{\omega + E_0 - \hat{H} + i\eta} \hat{\mathbf{B}}_i | \psi_0 \rangle \right], \quad (12)$$

where $\hat{\mathbf{B}}_i$ is defined in Eq. (6). The two local dynamical correlations share the similar behaviors including the

broad spectrum and the finite density in the zero frequency. Mostly significantly, the finite-size effects in the SLL phase is not manifest even though we use small clusters due to the limit of system size.

In the recent INS measurements on the triangular spin-liquid material YbMgGaO_4 ^{42,43,72}, the broad continuum spin excitations have been reported. While the high-energy spin excitations between 0.25 and 1.5 meV have been conjectured to be related with either a gapless spinon Fermi surface⁴² or the nearest-neighbor resonating valence bond correlations⁷², the low-energy excitations down to 0.02meV⁷² seem to include crucial information on the origin of the spin-liquid-like behaviors in the material, which is currently debated between an intrinsic spin liquid and a disorder-induced mimicry of a spin liquid^{42,43,45,46,48}. By considering the scenario of the disorder-induced spin-liquid-like phase, we compare our numerical results in the SLL phase with the INS data of YbMgGaO_4 . The SLL phase shows some similar behaviors of dynamical spin correlations with the experiment of YbMgGaO_4 , including the broadly spread spectral weights in the Brillouin zone and the suppressed spectral intensities near the Γ point⁴³. In the INS intensity data, the maxima at the K point above 0.5 meV shifts to the M point below 0.1 meV^{43,72}. The broad low-energy excitation maxima at the M point could be

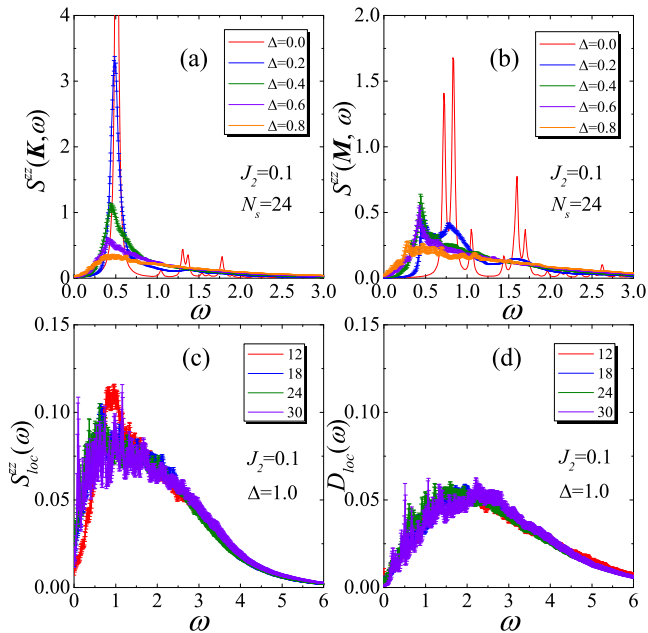


FIG. 7. (Color online) (a) and (b) are the dynamical structure factor at the K and the M points for $J_2 = 0.1$ on the 24-site torus system with different bond randomness strength. (c) and (d) are the momentum integrated dynamical spin and dimer correlations for $J_2 = 0.1, \Delta = 1.0$ in the SLL phase on different system sizes.

consistent with our SLL phase with a small J_2 coupling as shown in Fig. 6(d1).

Therefore, we identify a gapless SLL phase in the presence of strong bond randomness. In this SLL phase, we have not observed any conventional order or glass-type order. For further understanding on this phase, we calculate the sample distribution of spin correlation $\langle \hat{S}_i \hat{S}_j \rangle$ as shown in Fig. 8 (a). Interestingly, at larger distance side $r \geq 6$, the width of correlation distribution saturates to some finite value, which indicates the emergent long-range correlations between two spins with near equal probability of both positive and negative signs for different randomness configurations. To look into detail of nearest-neighbor correlation, we show the histogram of its distribution in Fig. 8 (b). Compared with 1D random singlet phase in bond randomness Heisenberg chain (see Appendix D), this distribution in the SLL phase shows a low probability near $-\frac{3}{4}J$. Different value of the next-nearest-neighbor J_2 would not change this behavior. The geometry frustration and the high coordination number $z = 6$ in the triangular lattice may play an important role here.

C. $J_1 - J_2$ spin liquid and the SLL phase

In this section, we study the difference between the $J_1 - J_2$ spin liquid and the SLL phase. In the absence of randomness, the nature of the $J_1 - J_2$ spin liquid is

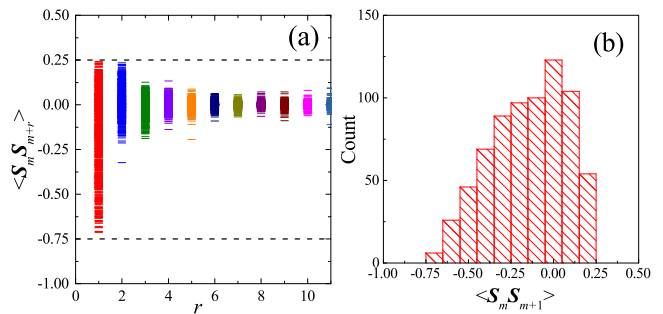


FIG. 8. (Color online) (a) Spin-spin correlations along the x direction on the YC6-24 cylinder. The reference site m is taken in the middle of the cylinder. r is the distance of the two sites along the x direction. We show the results of 720 independent random samples in the figure. The dashed lines show the lower and upper bound of spin-spin correlation. (b) The histogram of nearest-neighbor spin-spin correlation obtained from 720 independent random samples. We take 0.1 as the bar unit of the x axis. The y axis denotes the count number that the random sample gives the spin correlation value in the range of the given unit bar. Here, the next-nearest-neighbor interaction and bond randomness strength are chosen as $J_2 = 0.125, \Delta = 1.0$.

still debated between a gapless Dirac spin liquid and a gapped spin liquid^{52–57,71}. We calculate the triplet gap on the torus clusters up to 48 sites (see Appendix B), nonetheless the small-size data may not draw a conclusive evidence to show whether the gap is finite or not. If the gap is finite, we may expect a quantum phase transition from the gapped QSL to the gapless SLL phase, as suggested in Fig. 9. However, if the ED calculation suffers from strong finite-size effects and the spin liquid turns out to be gapless^{52,56}, our present size scaling may not correctly show the phase transition.

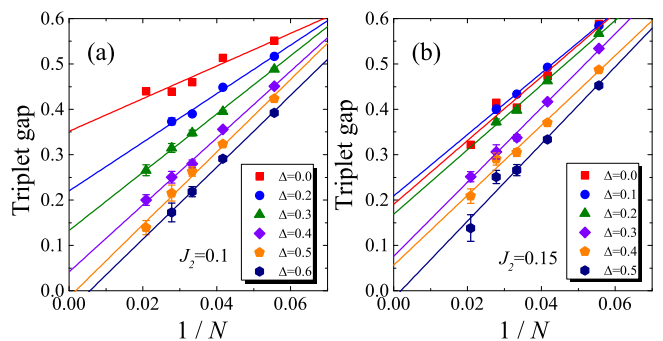


FIG. 9. (Color online) Linear size scaling of the spin triplet gap with inverse system size $1/N$ at (a) $J_2 = 0.1$ and $J_2 = 0.15$. We see the blend down behavior with growing randomness on finite-size system.

Since the QSL and the SLL state may have different entanglement structure, we calculate the entanglement spectrum on the cylinder geometry with two different open edges in the x direction. We denote the even bound-

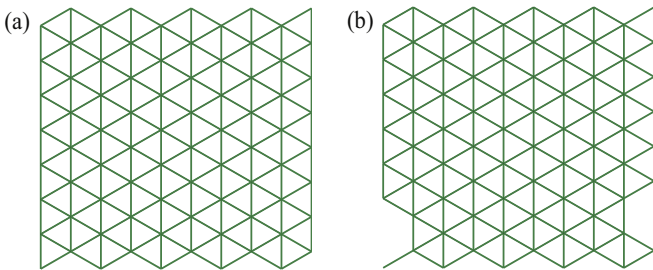


FIG. 10. (Color online) The YC8 cylinder with the even (a) and the odd (b) boundary conditions in the x direction. In the odd boundary condition (b), a spin-1/2 site is removed in each open edge.

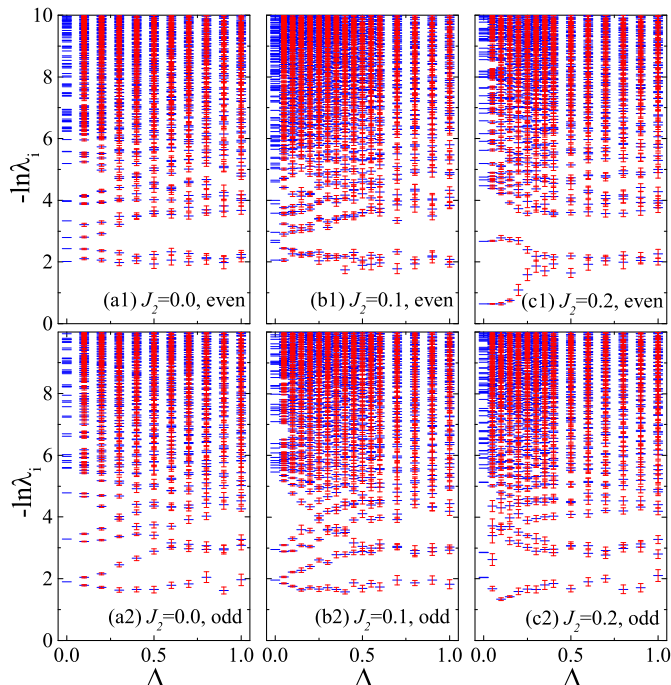


FIG. 11. (Color online) Entanglement spectra in the (a1-c1) even and (a2-c2) odd boundary conditions obtained on the YC8-24 cylinder using DMRG. λ_i are the eigenvalues of the reduced density matrix. The error bars are estimated from 15 independent randomness samples.

ary as the usual boundary conditions shown in Fig. 10(a) and the odd boundary by removing a spin-1/2 site on each open edge of the cylinder, as shown in Fig. 10(b). In Fig. 11, we show the entanglement spectra obtained on the YC8-24 cylinder. First of all, we analyze the spectrum in the SLL phase. In the even boundary shown in Figs. 11(a1,b1,c1), the spectrum always show a two-fold near degeneracy separated by a finite gap from the higher levels. The two-fold eigenvalues are identified as coming from the $S = 0$ and the $S = 1$ sectors (S is the good quantum number of total spin for the subsystem). In the odd boundary shown in Figs. 11(a2,b2,c2), one level with $S = 1/2$ and two levels with $S = 1/2, 3/2$ are found in

the low-lying spectrum. These features in both boundary conditions seem to be independent of J_2 for systems with large strength of the randomness, which might be used to characterize the SLL phase.

Next, we investigate the change of entanglement spectrum with randomness, starting from the $J_1 - J_2$ spin liquid. Since the characterization of the spin liquid phase in the even boundary conditions is likely to have large finite-size effects^{55,71}, here we consider the spectrum in the odd boundary conditions as shown in Fig. 11(b2). In the absence of randomness, the entanglement spectrum has a double degeneracy for all the eigenvalues^{54,55}. With increasing randomness, the two lowest eigenvalues split. For large randomness, we can see one level with $S = 1/2$ and two levels with $S = 1/2, 3/2$, which are separated from the higher spectrum. This feature for the SLL phase appears at $\Delta \sim 0.5$. We have also checked the entanglement spectrum of the YC6-24 cylinder and got the similar result as the YC8-24. In the kagome Heisenberg model, a possible phase transition induced by randomness between the clean kagome spin liquid and the SLL phase has been suggested at $\Delta \sim 0.4$ ³⁹, where the randomness sampling starts to have probability for the triplet ground state. In the ED calculation of the triangular model with $J_2 = 0.1$, we find probability for triplet ground state at $J_2 \gtrsim 0.6$, which is close to 0.5. The consistency between these different pictures suggests that the entanglement spectrum may be used as a characterization to distinguish the spin liquid and the SLL phase.

IV. SUMMARY AND DISCUSSION

By using the exact diagonalization (ED) and density matrix renormalization group (DMRG) techniques, we have studied the spin-1/2 $J_1 - J_2$ triangular Heisenberg model with bond randomness in both J_1 and J_2 couplings. In the absence of the randomness, the model has two magnetic order phases and a spin liquid phase between them⁵²⁻⁵⁷. This spin liquid phase may even extend to the anisotropic model that could be relevant to materials⁷³. By turning on the bond randomness, we find a randomness-induced spin-liquid-like (SLL) phase above a finite randomness strength Δ for a given J_2 , as shown in the phase diagram Fig. 1. This SLL phase does not show any spin, dimer, spin glass, or valence bond glass order in our finite-size scaling. The spin triplet and singlet gaps also seem to be vanishing after the finite-size scaling. These static properties suggest a gapless spin-liquid-like phase induced by bond randomness, which is supported by the dynamical spin structure factor $S^{zz}(\mathbf{q}, \omega)$. In the SLL phase, $S^{zz}(\mathbf{q}, \omega)$ shows a broad continuum in both momentum and frequency space. With growing J_2 , the broad maxima at the K point transfers its weight to the M point, showing that frustration affects short-range spin correlations even in presence of strong randomness. We compare the dynamical spin correlations of the SLL phase with the inelastic neutron scattering (INS) data of

the spin-liquid-like triangular material YbMgGaO_4 . The dynamical spectrum of the SLL phase with a small J_2 coupling could be consistent with the INS data of the low-energy excitations of YbMgGaO_4 , which shows the dominant broad maxima at the M point^{43,72}.

For studying randomness effects in the disordered $J_1 - J_2$ spin liquid, we examine the bipartite entanglement spectrum on cylinder geometry. We find the low-lying spectrum features in the SLL phase, which seems independent of J_2 and may characterize the random phase. This feature of entanglement spectrum appears at $\Delta \simeq 0.5$, which may suggest a phase transition from the spin liquid to the SLL phase and deserves more further studies. Before further discussion, we would like to remark that although most of our calculations are based on the ED method, we have pushed the system size as large as we can. Since the limit of system size, one should not interpret all the results as the final answer; however, we believe that our main results are convincing, including the gapless nonmagnetic behavior of the SLL phase, the absent glass-type orders, and the characteristic features of dynamical spin structure factor. In the absence of J_2 coupling, the bond randomness has been studied in previous ED calculation, which also proposed a spin-liquid-like phase with growing randomness¹⁴. Based on our phase diagram Fig. 1, it seems that the disordered phase extends to a large region with finite J_2 . No other disorder phase such as spin glass has been found.

Furthermore, we would like to discuss the nature of the SLL phase. In 2d systems, randomness may induce different quantum phases, with some examples such as a spin glass²⁹, VBG^{61,62}, and quantum Griffiths phase^{28,74}. These phases have been found in the diluted and random-graph-like systems, which are quite different from our model with bond coupling randomness and a perfect lattice geometry. For the SLL phase in this $J_1 - J_2$ triangular model, our results suggest that spin glass and VBG phases are unlikely. The numerical SDRG analysis for frustrated Heisenberg models suggested a spin glass fixed point³⁷, which however seems not consistent with our result and the recent numerical studies on other frustrated models^{14,36,38,39}. In a recent theoretical paper by I. Kimchi et. al., the authors have studied the effects of bond randomness on 2d valence bond solid and spin liquid states⁴⁸. They found that the bond randomness inevitably leads to the nucleation of topological defects with spin-1/2 when destructing the valence bond order, which would yield gapless spin excitations and the short-ranged VBG order would be unstable. The SLL phase found in our numerical calculation, which shows gapless spin excitations and vanished VBG order, appears to be in agreement with the proposed state in Ref. 48. The next check of this SLL phase could be the thermodynamic properties such as specific heat and susceptibility, which we leave for future study.

Finally, we would like to make some remarks about the application of our results to experiments. For YbMgGaO_4 , bond randomness may not be weak⁴⁴, and

second-neighbor interaction may play an important role for the observations of experiments⁴³. Theoretical calculations found that the spin anisotropic interactions may not drive a spin-liquid-like behavior but support magnetic ordering^{45,46}. By considering a minimum model to study the effects of competing interaction and disorder, we find that the dynamical structure factor of the spin-liquid-like phase with a small J_2 agrees with the INS data of YbMgGaO_4 . The gapless excitations and the absence of the spin glass order are also consistent with experimental observations. All these results indicate a consistent description of the spin-liquid-like phase on the ground state of YbMgGaO_4 from our minimum model. In this $J_1 - J_2$ model, we do not find a spin glass order in the presence of bond randomness. For understanding the spin-glass-like freezing in materials such as YbZnGaO_4 ⁵⁰, other spin anisotropic couplings may play important roles, which deserves further study.

Note added. Recently, we became aware of an interesting work⁷⁵, which studied a spin-1/2 J-Q model on the square lattice with bond randomness using quantum Monte Carlo. The authors also found a disorder-induced spin-liquid-like phase, which was suggested as a random singlet phase.

ACKNOWLEDGMENTS

D.N.S thanks Leon Balents for suggesting of the problem. We thank Wen-An Guo, Dao-Xin Yao, Rong-Qiang He, and Zi Yang Meng for fruitful discussions. We also acknowledge extensive discussions with Itamar Kimchi. H. Q. W would like to thank Wei Zhu for helpful discussions about block-diagonalization using symmetries. H. Q. W also would like to thank the Magic-II platform at Shanghai Supercomputer Center. This research is supported by National Science Foundation Grants PREM DMR-1828019 (H.Q.W.) and DMR-1408560 (D.N.S.). S.S.G. is supported by the National Natural Science Foundation of China Grants 11834014, 11874078, and the start-up funding support from Beihang University.

Appendix A: Finite-size clusters

In this paper, we use both ED and DMRG to do the tori calculations. These tori are made of two dimension clusters (which are shown in Fig. 12) under periodic boundary conditions. In order to get unbiased extrapolations, the geometries of tori are important. Since 120° Neel order and stripe order are the two competing magnetic phases, they need to be considered on an equal footing. Therefore, almost all of geometries (except for the 48-site one) we chose are commensurate to the 120° antiferromagnetic order, i.e. they have two K momentum points in the Brillouin zone (BZ). And all the clusters with even sites are also commensurate to the collinear or stripe order. We also note that the 36-site and 48-site

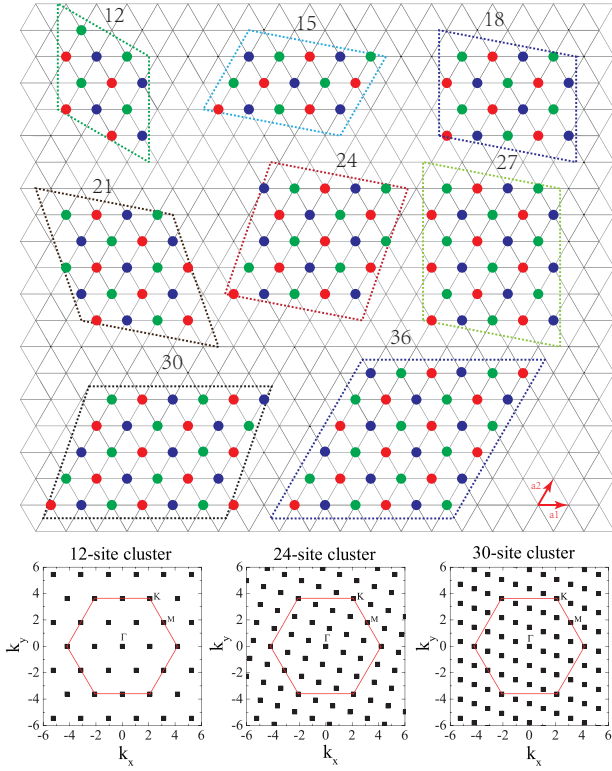


FIG. 12. Most of finite-size clusters used in the numerical calculations. The red, green and olive solid points represent three sublattices of 120° AF order or $\sqrt{3} \times \sqrt{3}$ magnetic order. $\mathbf{a}_1 = (a, 0)$ and $\mathbf{a}_2 = (a/2, \sqrt{3}a/2)$ are primitive vectors. Here we set the lattice constant or nearest-neighbor bond length $a = 1$ as unit of length. The dashed lines which connect the bond centers of the triangular lattice in the 24-site cluster form a Kagome lattice. The bottom three figures show the finite-size points in momentum space. In addition, 18- and 48- site rhombic clusters can be easily obtained by expanding 6×3 and 8×6 primitive cells. The 18-site rhombic cluster has been used in the calculation of singlet and triplet gaps in Fig. 14 and Fig. 15.

clusters have both three M points in the BZ, while other clusters with even sites only have one M point in the BZ. As a consequence of that, the square sublattice magnetization for stripe phase on 36-site torus is overestimate than other system sizes (like 18, 24, 30), as can be seen in Fig. 2 of main text. One should also note that the 24-site cluster we use here is different from those in Ref. 39.

For the tori smaller or equal to 30 sites, we use exact diagonalization to do the calculations. While for 36-site and 48-site clusters, we use SU(2) DMRG by keeping as many as 8000 U(1)-equivalent states to do the calculations. The truncation errors are less than 5×10^{-5} in all calculations.

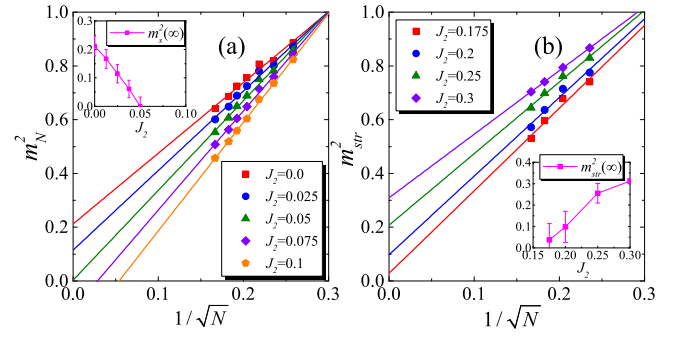


FIG. 13. Linear finite-size scaling of square magnetization of (a) 120° AF order and (b) stripe AF order versus $1/\sqrt{N}$ at various next-nearest-neighbor interaction J_2 . The insets are the extrapolated values in the thermodynamic limit.

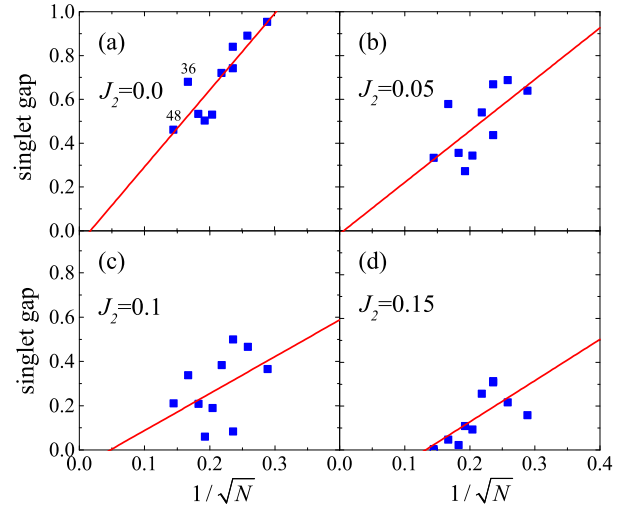


FIG. 14. Linear extrapolation of singlet gaps with $1/\sqrt{N}$ at various J_2 . The solid lines are least-square fitting lines. The singlet gaps all seem to be zero in the thermodynamic limit.

Appendix B: $J_1 - J_2$ Triangular Heisenberg model

We have used finite-size tori to study the non-randomness $J_1 - J_2$ Heisenberg model on triangular lattice. Using linear extrapolation of magnetic order parameters, we got the nonmagnetic region which is about $0.05(1) < J_2 < 0.16(2)$. This phase region is similar to the previous DMRG results^{54,55} and is larger than the VMC results⁵².

Both the 120° AF phase and Stripe AF phase spontaneously break the spin SU(2) continuous symmetry in the thermodynamic limit. According to Nambu-Goldstone theorem, the system in these magnetic phase regions has gapless excitations. In finite-size systems, a characteristic and systematic structure of the continuous symmetry breaking is the Anderson tower of states (TOS) in the energy spectrum. The TOS energy levels scales with $1/N$ to the ground state, while the low energy magnon exci-

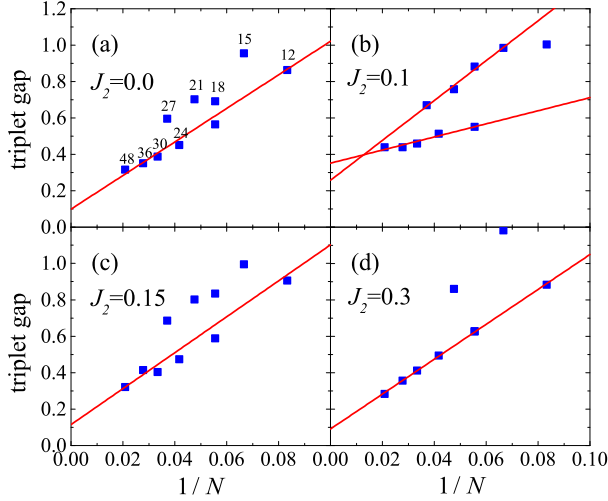


FIG. 15. Triplet gaps scale with $1/N$ at various J_2 . The solid lines in (a) and (c) are least-square fitting lines using even-size tori. The dashed line in (d) is the cubic-polynomial fitting lines. At $J_2 = 0.1$, we use two groups of data to do the fitting and ignore the small 12-site torus. Two 18-site tori are used here, one is illustrated in Fig. 12; the other is a rhombic cluster expanded by 6×3 primitive cells. The 18-site rhombic cluster has smaller triplet gaps than the nonrhombic one.

tations scale with $1/\sqrt{N}$ (or $1/L$, L is the linear system size). Based on the knowledge, we scale the singlet gap with $1/\sqrt{N}$ and triplet gap with $1/N$. N is the number of lattice sites.

In the $SU(2)$ symmetry breaking phases, the singlet and triplet gaps should go to zero in the thermodynamic limit in the magnetic regions. From our finite-size calculations, though some data has large variance, we still can see the gapless tendency in Fig. 14 (a-b) and Fig. 15 (a) and (d). Unfortunately, the system size is still not large enough to unbiasedly extrapolate the triplet gap to zero in the finite-size scaling. For the nonmagnetic phase [Fig. 14 (c-d) and Fig. 15 (b-c)], it is even harder to draw a conclusion whether it is gapless or not using the finite-size clusters and the linear extrapolation.

Appendix C: Dimer correlation

In this sector, we show some dimer-dimer correlation function in momentum space. In order to see the possible off-diagonal valence bond solid pattern, we take every bond as a new lattice site which is sitting in the middle of each bond. These new sites form a kagome lattice ($1/4$ -depleted triangular lattice, dashed lines in Fig. 12) or with $3N$ lattice sites, N is the number of sites in the original triangular lattice. Then we take the Fourier transform from real space to momentum space using Eq. (6). Here, we show the contour plot of dimer correlation in momentum space using 24-site cluster, which is shown in Fig. 16. We take the maximum $D(X)$ to do the structure

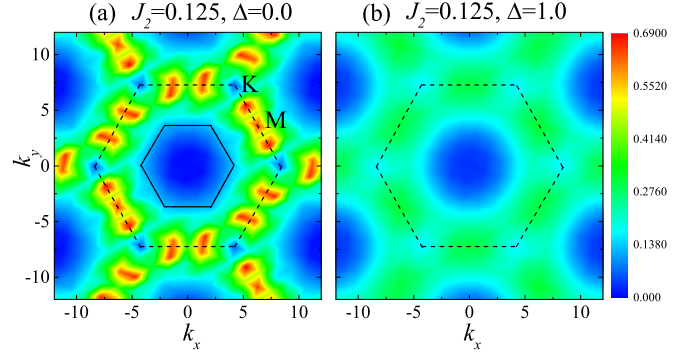


FIG. 16. Contour plot of dimer correlation in momentum space at $J_1 = 0.125$, $\Delta = 0.0$ and $J_1 = 0.125$, $\Delta = 1.0$.

factor scaling. X is the momentum site where $D(\mathbf{q})$ takes its maximum. And it is the same or close to the middle point in between K and M points [see Fig. 16 (a)] depending on the geometry of the finite-size clusters. There is no any pattern of long-range VBS order in our numerical study (see Fig. 3 in the main text). In Fig. 16 (a), the solid hexagon is the Brillouin zone edge of original triangular lattice with N sites, while the dashed hexagon is the “Brillouin zone” edge of new depleted triangular lattice with $3N$ sites.

Appendix D: Histogram of spin correlations under different bond randomness strength

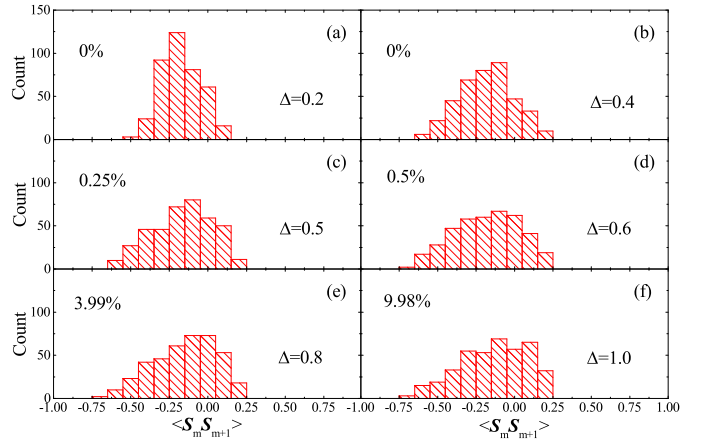


FIG. 17. Histograms of nearest-neighbor spin correlation with different bond randomness strength Δ . The finite-size system we take is 24-site torus with 400 independent disorder configurations. And the next-nearest-neighbor exchange interaction J_2 is set to be $0.125J_1$. The percentages shown in the boxes mean the proportions of triplet ground state under 400 disorder configurations.

Here, we want to show how the distribution of nearest-neighbor spin correlation changes with the bond randomness strength. As the bond randomness strength in-

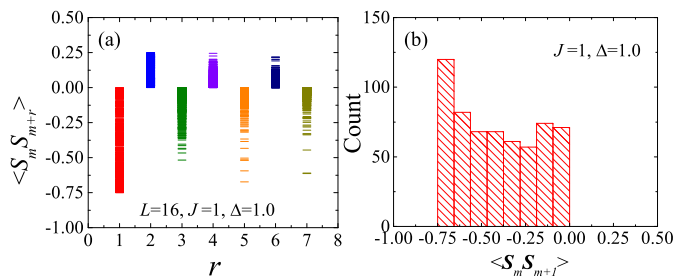


FIG. 18. (a) Spin-spin correlations (with distributions) at different distances on the $L = 16$ Heisenberg chain with bond randomness $\Delta = 1.0$. The logarithmic corrections to the power-law decaying correlations have been found in recent quantum Monte Carlo simulations²⁶. (b) The histogram of nearest-neighbor spin-spin correlation obtained from 600 independent random samples. Two nearest-neighbor spins have a large probability to form a singlet with the correlations trend to be $-\frac{3}{4}J$.

creases, the distribution of n.n. spin correlation becomes broaden and extends to $-\frac{3}{4}J$ and $\frac{1}{4}J$. Also, the distribution changes from a gaussian-like shape to a asymmetric one. However, it is a rare event to be a (approximated) singlet between two nearest-neighbor sites. It is an striking difference between 1D random singlet phase and the SLL phase. In 1D RS phase, the n.n. spin correlation has large probability to be $-\frac{3}{4}J$ in Fig. 18.

* shoushu.gong@buaa.edu.cn

† donna.sheng1@csun.edu

¹ Claudine Lacroix, Philippe Mendels, and Frederic Mila, “Introduction to frustrated magnetism: Materials, experiments, theory,” Springer (2013).

² Leon Balents, “Spin liquids in frustrated magnets,” *Nature* **464**, 199–208 (2010).

³ Lucile Savary and Leon Balents, “Quantum spin liquids: a review,” *Reports on Progress in Physics* **80**, 016502 (2016).

⁴ M. R. Norman, “Colloquium,” *Rev. Mod. Phys.* **88**, 041002 (2016).

⁵ Yi Zhou, Kazushi Kanoda, and Tai-Kai Ng, “Quantum spin liquid states,” *Rev. Mod. Phys.* **89**, 025003 (2017).

⁶ X. G. Wen, “Mean-field theory of spin-liquid states with finite energy gap and topological orders,” *Phys. Rev. B* **44**, 2664–2672 (1991).

⁷ N. Read and Subir Sachdev, “Large- n expansion for frustrated quantum antiferromagnets,” *Phys. Rev. Lett.* **66**, 1773–1776 (1991).

⁸ Xie Chen, Zheng-Cheng Gu, and Xiao-Gang Wen, “Local unitary transformation, long-range quantum entanglement, wave function renormalization, and topological order,” *Phys. Rev. B* **82**, 155138 (2010).

⁹ Y. Shimizu, K. Miyagawa, K. Kanoda, M. Maesato, and G. Saito, “Spin liquid state in an organic mott insulator with a triangular lattice,” *Phys. Rev. Lett.* **91**, 107001 (2003).

¹⁰ Y. Kurosaki, Y. Shimizu, K. Miyagawa, K. Kanoda, and G. Saito, “Mott transition from a spin liquid to a fermi liquid in the spin-frustrated organic conductor κ -(ET)₂Cu₂(CN)₃,” *Phys. Rev. Lett.* **95**, 177001 (2005).

¹¹ Satoshi Yamashita, Yasuhiro Nakazawa, Masaharu Oguni, Yugo Oshima, Hiroyuki Nojiri, Yasuhiro Shimizu, Kazuya Miyagawa, and Kazushi Kanoda, “Thermodynamic properties of a spin-1/2 spin-liquid state in a -type organic salt,” *Nature Physics* **4**, 459 (2008).

¹² Minoru Yamashita, Norihito Nakata, Yuichi Kasahara, Takahiko Sasaki, Naoki Yoneyama, Norio Kobayashi, Satoshi Fujimoto, Takasada Shibauchi, and Yuji Mat-

suda, “Thermal-transport measurements in a quantum spin-liquid state of the frustrated triangular magnet - (bedt-ttf)₂cu₂(cn)₃,” *Nature Physics* **5**, 44 (2008).

¹³ Minoru Yamashita, Norihito Nakata, Yoshinori Senshu, Masaki Nagata, Hiroshi M. Yamamoto, Reizo Kato, Takasada Shibauchi, and Yuji Matsuda, “Highly mobile gapless excitations in a two-dimensional candidate quantum spin liquid,” *Science* **328**, 1246–1248 (2010).

¹⁴ Ken Watanabe, Hikaru Kawamura, Hiroki Nakano, and Toru Sakai, “Quantum spin-liquid behavior in the spin-1/2 random heisenberg antiferromagnet on the triangular lattice,” *Journal of the Physical Society of Japan* **83**, 034714 (2014).

¹⁵ Danna E. Freedman, Tianheng H. Han, Andrea Prodi, Peter Mller, Qing-Zhen Huang, Yu-Sheng Chen, Samuel M. Webb, Young S. Lee, Tyrel M. McQueen, and Daniel G. Nocera, “Site specific x-ray anomalous dispersion of the geometrically frustrated kagom magnet, herbertsmithite, zncu₃(oh)6cl₂,” *Journal of the American Chemical Society* **132**, 16185 (2010).

¹⁶ Lucile Savary and Leon Balents, “Disorder-induced quantum spin liquid in spin ice pyrochlores,” *Phys. Rev. Lett.* **118**, 087203 (2017).

¹⁷ Shang-keng Ma, Chandan Dasgupta, and Chin-kun Hu, “Random antiferromagnetic chain,” *Phys. Rev. Lett.* **43**, 1434–1437 (1979).

¹⁸ Chandan Dasgupta and Shang-keng Ma, “Low-temperature properties of the random heisenberg antiferromagnetic chain,” *Phys. Rev. B* **22**, 1305–1319 (1980).

¹⁹ Daniel S. Fisher, “Random transverse field ising spin chains,” *Phys. Rev. Lett.* **69**, 534–537 (1992).

²⁰ Daniel S. Fisher, “Random antiferromagnetic quantum spin chains,” *Phys. Rev. B* **50**, 3799–3821 (1994).

²¹ R. N. Bhatt and P. A. Lee, “Scaling studies of highly disordered spin-1/2 antiferromagnetic systems,” *Phys. Rev. Lett.* **48**, 344–347 (1982).

²² R. Mélin, Y.-C. Lin, P. Lajkó, H. Rieger, and F. Iglói, “Strongly disordered spin ladders,” *Phys. Rev. B* **65**,

- 104415 (2002).
- ²³ Gil Refael, Stefan Kehrein, and Daniel S. Fisher, “Spin reduction transition in spin- $\frac{3}{2}$ random heisenberg chains,” *Phys. Rev. B* **66**, 060402 (2002).
- ²⁴ G. Refael and J. E. Moore, “Entanglement entropy of random quantum critical points in one dimension,” *Phys. Rev. Lett.* **93**, 260602 (2004).
- ²⁵ V. L. Quito, José A. Hoyos, and E. Miranda, “Emergent $su(3)$ symmetry in random spin-1 chains,” *Phys. Rev. Lett.* **115**, 167201 (2015).
- ²⁶ Yu-Rong Shu, Dao-Xin Yao, Chih-Wei Ke, Yu-Cheng Lin, and Anders W. Sandvik, “Properties of the random-singlet phase: From the disordered heisenberg chain to an amorphous valence-bond solid,” *Phys. Rev. B* **94**, 174442 (2016).
- ²⁷ Yu-Rong Shu, Maxime Dupont, Dao-Xin Yao, Sylvain Capponi, and Anders W. Sandvik, “Dynamical properties of the $s = \frac{1}{2}$ random heisenberg chain,” *Phys. Rev. B* **97**, 104424 (2018).
- ²⁸ Robert B. Griffiths, “Nonanalytic behavior above the critical point in a random ising ferromagnet,” *Phys. Rev. Lett.* **23**, 17–19 (1969).
- ²⁹ K. Binder and A. P. Young, “Spin glasses: Experimental facts, theoretical concepts, and open questions,” *Rev. Mod. Phys.* **58**, 801–976 (1986).
- ³⁰ Yoseph Imry and Shang-keng Ma, “Random-field instability of the ordered state of continuous symmetry,” *Phys. Rev. Lett.* **35**, 1399–1401 (1975).
- ³¹ Olexei Motrunich, Siun-Chuon Mau, David A. Huse, and Daniel S. Fisher, “Infinite-randomness quantum ising critical fixed points,” *Phys. Rev. B* **61**, 1160–1172 (2000).
- ³² István A. Kovács and Ferenc Iglói, “Infinite-disorder scaling of random quantum magnets in three and higher dimensions,” *Phys. Rev. B* **83**, 174207 (2011).
- ³³ Thomas Vojta, Adam Farquhar, and Jason Mast, “Infinite-randomness critical point in the two-dimensional disordered contact process,” *Phys. Rev. E* **79**, 011111 (2009).
- ³⁴ Thomas Vojta, Chetan Kotabage, and José A. Hoyos, “Infinite-randomness quantum critical points induced by dissipation,” *Phys. Rev. B* **79**, 024401 (2009).
- ³⁵ Nicolas Laflorencie, Stefan Wessel, Andreas Läuchli, and Heiko Rieger, “Random-exchange quantum heisenberg antiferromagnets on a square lattice,” *Phys. Rev. B* **73**, 060403 (2006).
- ³⁶ Kazuki Uematsu and Hikaru Kawamura, “Randomness-induced quantum spin liquid behavior in the $s = 1/2$ random j_1 - j_2 heisenberg antiferromagnet on the honeycomb lattice,” *Journal of the Physical Society of Japan* **86**, 044704 (2017).
- ³⁷ Y.-C. Lin, R. Mélin, H. Rieger, and F. Iglói, “Low-energy fixed points of random heisenberg models,” *Phys. Rev. B* **68**, 024424 (2003).
- ³⁸ Hikaru Kawamura, Ken Watanabe, and Tokuro Shimokawa, “Quantum spin-liquid behavior in the spin-1/2 random-bond heisenberg antiferromagnet on the kagome lattice,” *Journal of the Physical Society of Japan* **83**, 103704 (2014).
- ³⁹ Tokuro Shimokawa, Ken Watanabe, and Hikaru Kawamura, “Static and dynamical spin correlations of the $s = \frac{1}{2}$ random-bond antiferromagnetic heisenberg model on the triangular and kagome lattices,” *Phys. Rev. B* **92**, 134407 (2015).
- ⁴⁰ Y. Li, H. Liao, Z. Zhang, S. Li, F. Jin, L. Ling, L. Zhang, Y. Zou, L. Pi, Z. Yang, J. Wang, Z. Wu, and Q. Zhang, “Gapless quantum spin liquid ground state in the two-dimensional spin-1/2 triangular antiferromagnet $ybm\text{ggao}_4$,” *Scientific Reports* **5**, 16419 (2015).
- ⁴¹ Yuesheng Li, Gang Chen, Wei Tong, Li Pi, Juanjuan Liu, Zhaorong Yang, Xiaoqun Wang, and Qingming Zhang, “Rare-earth triangular lattice spin liquid: A single-crystal study of $ybm\text{ggao}_4$,” *Phys. Rev. Lett.* **115**, 167203 (2015).
- ⁴² Yao Shen, Yao-Dong Li, Hongliang Wo, Yuesheng Li, Shoudong Shen, Bingying Pan, Qisi Wang, H. C. Walker, P. Steffens, M. Boehm, Yiqing Hao, D. L. Quintero-Castro, L. W. Harriger, M. D. Frontzek, Lijie Hao, Siqin Meng, Qingming Zhang, Gang Chen, and Jun Zhao, “Evidence for a spinon fermi surface in a triangular-lattice quantum-spin-liquid candidate,” *Nature* **540**, 559 (2016).
- ⁴³ Joseph A. M. Paddison, Marcus Daum, Zhiling Dun, Georg Ehlers, Yaohua Liu, Matthew B. Stone, Haidong Zhou, and Martin Mourigal, “Continuous excitations of the triangular-lattice quantum spin liquid $ybm\text{ggao}_4$,” *Nature Physics* **13**, 117 (2016).
- ⁴⁴ Yuesheng Li, Devashibhai Adroja, Robert I. Bewley, David Voneshen, Alexander A. Tsirlin, Philipp Gegenwart, and Qingming Zhang, “Crystalline electric-field randomness in the triangular lattice spin-liquid $ybm\text{ggao}_4$,” *Phys. Rev. Lett.* **118**, 107202 (2017).
- ⁴⁵ Qiang Luo, Shijie Hu, Bin Xi, Jize Zhao, and Xiaoqun Wang, “Ground-state phase diagram of an anisotropic spin- $\frac{1}{2}$ model on the triangular lattice,” *Phys. Rev. B* **95**, 165110 (2017).
- ⁴⁶ Zhenyue Zhu, P. A. Maksimov, Steven R. White, and A. L. Chernyshev, “Disorder-induced mimicry of a spin liquid in $ybm\text{ggao}_4$,” *Phys. Rev. Lett.* **119**, 157201 (2017).
- ⁴⁷ Jason Iaconis, Chunxiao Liu, Gbor B. Halsz, and Leon Balents, “Spin Liquid versus Spin Orbit Coupling on the Triangular Lattice,” *SciPost Phys.* **4**, 003 (2018).
- ⁴⁸ Itamar Kimchi, Adam Nahum, and T. Senthil, “Valence bonds in random quantum magnets: Theory and application to $ybm\text{ggao}_4$,” *Phys. Rev. X* **8**, 031028 (2018).
- ⁴⁹ Edward Parker and Leon Balents, “Finite-temperature behavior of a classical spin-orbit-coupled model for $ybm\text{ggao}_4$ with and without bond disorder,” *Phys. Rev. B* **97**, 184413 (2018).
- ⁵⁰ Zhen Ma, Jinghui Wang, Zhao-Yang Dong, Jun Zhang, Shichao Li, Shu-Han Zheng, Yunjie Yu, Wei Wang, Liqiang Che, Kejing Ran, Song Bao, Zhengwei Cai, P. Čermák, A. Schneidewind, S. Yano, J. S. Gardner, Xin Lu, Shun-Li Yu, Jun-Ming Liu, Shiyang Li, Jian-Xin Li, and Jinsheng Wen, “Spin-glass ground state in a triangular-lattice compound $ybzngao_4$,” *Phys. Rev. Lett.* **120**, 087201 (2018).
- ⁵¹ Xinshu Zhang, Fahad Mahmood, Marcus Daum, Zhiling Dun, Joseph A. M. Paddison, Nicholas J. Laurita, Tao Hong, Haidong Zhou, N. P. Armitage, and Martin Mourigal, “Hierarchy of exchange interactions in the triangular-lattice spin liquid $ybm\text{ggao}_4$,” *Phys. Rev. X* **8**, 031001 (2018).
- ⁵² Ryui Kaneko, Satoshi Morita, and Masatoshi Imada, “Gapless spin-liquid phase in an extended spin 1/2 triangular heisenberg model,” *Journal of the Physical Society of Japan* **83**, 093707 (2014).
- ⁵³ P. H. Y. Li, R. F. Bishop, and C. E. Campbell, “Quasi-classical magnetic order and its loss in a spin- $\frac{1}{2}$ heisenberg antiferromagnet on a triangular lattice with competing bonds,” *Phys. Rev. B* **91**, 014426 (2015).
- ⁵⁴ Zhenyue Zhu and Steven R. White, “Spin liquid phase of

- the $s = \frac{1}{2} j_1 - j_2$ heisenberg model on the triangular lattice,” *Phys. Rev. B* **92**, 041105 (2015).
- ⁵⁵ Wen-Jun Hu, Shou-Shu Gong, Wei Zhu, and D. N. Sheng, “Competing spin-liquid states in the spin- $\frac{1}{2}$ heisenberg model on the triangular lattice,” *Phys. Rev. B* **92**, 140403 (2015).
- ⁵⁶ Yasir Iqbal, Wen-Jun Hu, Ronny Thomale, Didier Poilblanc, and Federico Becca, “Spin liquid nature in the heisenberg $J_1 - J_2$ triangular antiferromagnet,” *Phys. Rev. B* **93**, 144411 (2016).
- ⁵⁷ S. N. Saadatmand and I. P. McCulloch, “Symmetry fractionalization in the topological phase of the spin- $\frac{1}{2}$ $J_1 - J_2$ triangular heisenberg model,” *Phys. Rev. B* **94**, 121111 (2016).
- ⁵⁸ Steven R. White, “Density matrix formulation for quantum renormalization groups,” *Phys. Rev. Lett.* **69**, 2863–2866 (1992).
- ⁵⁹ IP McCulloch and M Gulácsi, “The non-abelian density matrix renormalization group algorithm,” *Europhysics Letters* **57**, 852–858 (2002).
- ⁶⁰ Herbert Neuberger and Timothy Ziman, “Finite-size effects in heisenberg antiferromagnets,” *Phys. Rev. B* **39**, 2608–2618 (1989).
- ⁶¹ M. Tarzia and G. Biroli, “The valence bond glass phase,” *EPL (Europhysics Letters)* **82**, 67008 (2008).
- ⁶² R. R. P. Singh, “Valence bond glass phase in dilute kagome antiferromagnets,” *Phys. Rev. Lett.* **104**, 177203 (2010).
- ⁶³ Y. Nonomura and Y. Ozeki, “Ground-State Phase Diagrams of the Two-Dimensional Quantum Heisenberg Spin Glass Models,” *Journal of the Physical Society of Japan* **64**, 2710 (1995).
- ⁶⁴ J. Oitmaa and O. P. Sushkov, “Two-dimensional randomly frustrated spin-1/2 heisenberg model,” *Phys. Rev. Lett.* **87**, 167206 (2001).
- ⁶⁵ Creighton K. Thomas, David A. Huse, and A. A. Middleton, “Zero- and low-temperature behavior of the two-dimensional $\pm j$ ising spin glass,” *Phys. Rev. Lett.* **107**, 047203 (2011).
- ⁶⁶ Shanon J. Rubin, Na Xu, and Anders W. Sandvik, “Dual time scales in simulated annealing of a two-dimensional ising spin glass,” *Phys. Rev. E* **95**, 052133 (2017).
- ⁶⁷ Yining Xu and Dao-Xin Yao, “Spin glass in the bond-diluted $J_1 - J_2$ ising model on the square lattice,” *Phys. Rev. B* **97**, 224419 (2018).
- ⁶⁸ Cornelius Lanczos, “An iteration method for the solution of the eigenvalue problem of linear differential and integral operators,” *J. Research Nat. Bur. Standards* **45**, 255–282 (1950).
- ⁶⁹ Y. Saad, *Numerical Methods for Large Eigenvalue Problems* (Society for Industrial and Applied Mathematics, 2011) <http://epubs.siam.org/doi/pdf/10.1137/1.9781611970739>.
- ⁷⁰ E. R. Gagliano and C. A. Balseiro, “Dynamical properties of quantum many-body systems at zero temperature,” *Phys. Rev. Lett.* **59**, 2999–3002 (1987).
- ⁷¹ Shou-Shu Gong, W. Zhu, J.-X. Zhu, D. N. Sheng, and Kun Yang, “Global phase diagram and quantum spin liquids in a spin- $\frac{1}{2}$ triangular antiferromagnet,” *Phys. Rev. B* **96**, 075116 (2017).
- ⁷² Yuesheng Li, Devashibhai Adroja, David Voneshen, Robert I. Bewley, Qingming Zhang, Alexander A. Tsirlin, and Philipp Gegenwart, “Nearest-neighbour resonating valence bonds in ybmgao4,” *Nature Communications* **8**, 15814 (2017).
- ⁷³ Zhenyue Zhu, P. A. Maksimov, Steven R. White, and A. L. Chernyshev, “Topography of spin liquids on a triangular lattice,” *Phys. Rev. Lett.* **120**, 207203 (2018).
- ⁷⁴ Rong Yu, Tommaso Roscilde, and Stephan Haas, “Quantum disorder and griffiths singularities in bond-diluted two-dimensional heisenberg antiferromagnets,” *Phys. Rev. B* **73**, 064406 (2006).
- ⁷⁵ Lu Liu, Hui Shao, Yu-Cheng Lin, Wenan Guo, and Anders W. Sandvik, “Random-singlet phase in disordered two-dimensional quantum magnets,” *arXiv* **1804**, 06108 (2018).